Available online at www.sciencedirect.com
ScienceDirect
Applied Surface Science 253 (2007) 4490–4496
applied surface science
www.elsevier.com/locate/apsusc

Characterization of microarc oxidation coatings formed on AM60B magnesium alloy in silicate and phosphate electrolytes

Jun Liang [a,b], Litian Hu [a], Jingcheng Hao [a,*]

[a] State Key Laboratory of Solid Lubrication, Lanzhou Institute of Chemical Physics, Chinese Academy of Sciences, Lanzhou 730000, PR China
[b] Graduate School of Chinese Academy of Sciences, Beijing 100039, PR China

Received 27 April 2006; received in revised form 29 September 2006; accepted 30 September 2006
Available online 30 January 2007

Abstract

Microarc oxidation coatings on AM60B magnesium alloy were prepared in silicate and phosphate electrolytes. Structure, composition, mechanical property, tribological, and corrosion resistant characteristics of the coatings was studied by scanning electron microscope (SEM), X-ray diffraction (XRD) and microhardness analyses, and by ball-on-disc friction and potentiodynamic corrosion testing. It is found that the coating produced from the silicate electrolyte is compact and uniform and is mainly composed of MgO and forsterite Mg_2SiO_4 phases, while the one formed in phosphate electrolyte is relatively porous and is mainly composed of MgO phase. The thick coating produced from a silicate electrolyte possesses a high hardness and provides a low wear rate (3.55×10^{-5} mm^3/Nm) but a high friction coefficient against Si_3N_4 ball. A relatively low hardness and friction coefficient while a high wear rate (8.65×10^{-5} mm^3/Nm) is recorded during the testing of the thick coating produced from a phosphate electrolyte. Both of these types of coatings provide effective protection for the corrosion resistance compared with the uncoated magnesium alloy. The coating prepared from the silicate electrolyte demonstrates better corrosion behavior due to the compacter microstructure.

Keywords: Magnesium alloy; Microarc oxidation; Oxide coating; Friction and wear; Corrosion resistance

1. Introduction

It is known that magnesium is the lightest of the currently used construction metals [1]. Moreover, magnesium alloys have high strength to weight ratio, high dimensional stability, good electromagnetic shielding and damping characteristics, and are easy to machine and recycle. Thus, its application is becoming attractive especially for aerospace, automotive and communication fields. However, the main factors limiting the application of Mg alloys are their comparatively low corrosion and wear resistance [2,3]. One of the most effective ways to overcome these problems is to coat the base material. There are a number of possible coating technologies to be available for magnesium and its alloy including electrochemical plating, conversion coatings, anodizing, gas-phase deposition processes, laser surface alloying and organic coatings [2]. Of these techniques, anodizing is one of most popular method [4,5]. Microarc oxidation (MAO), as a relatively new surface treatment technique based on the traditional anodic oxidation, has been attracting greatly interest in recent years, because MAO can remarkably enhance the corrosion and wear resistance by producing a relatively thick, dense and hard film [6,7].

Much research has highlighted the significant role which the electrolyte plays in the MAO process and in providing the surface of magnesium and its alloys with the desired coating. Thus, in general, the nature and properties of the coatings formed on magnesium and its alloys depends, to a great extent, on the composition of the electrolyte [8,9]. Alkaline phosphate and silicate electrolytes were used as the base electrolytes to produce oxide coatings on magnesium and its alloys [5,10–12]. However, up to now, there is only limited information about the effect of these two types of base electrolytes on the formation behavior and the structure and properties of oxide coating formed on magnesium alloys. In the present work, the kinetics of constant current density microarc oxidation as well as the morphology, structure, and composition of oxide coatings formed in silicate and phosphate base electrolytes were investigated. The mechanical, tribological and anti-corrosive properties of the oxide coatings were also evaluated.

* Corresponding author. Tel.: +86 931 4968173.
E-mail addresses: liangjun9@yahoo.com.cn (J. Liang), jhao@sdu.edu.cn (J. Hao).

0169-4332/$ – see front matter © 2006 Elsevier B.V. All rights reserved.
doi:10.1016/j.apsusc.2006.09.064

Table 1
Process parameters of microarc oxidation in different electrolytes

Electrolyte	Composition	Conductivity of electrolyte (mS/cm)	Breakdown voltage (V)	Final voltage (V)
Silicate	10.0 g/L Na_2SiO_3 + 1.0 g/L KOH	12.9	200 ± 5	505 ± 5
Phosphate	10.0 g/L Na_3PO_4 + 1.0 g/L KOH	8.8	255 ± 5	520 ± 5

2. Experimental

2.1. Preparation of microarc oxidation coatings

Panel substrates made of AM60B Mg alloy with a size of 20 mm × 36 mm × 2 mm (mass fraction: Al 5.6–6.4%, Mn 0.26–0.4%, Zn ≤ 0.2%, balance Mg) were ground and polished with SiC abrasive paper to obtain an average surface roughness of $R_a \approx 0.18$ μm. The microarc oxidation processes were conducted on a WHYH-20 high-power pulsed bi-polar electrical source, a stainless steel container with a sample-holder as the electrolyte cell, and a stirring and cooling system. Aqueous electrolytes were prepared from solutions of Na_2SiO_3, or Na_3PO_4 (10.0 g/L) in distilled water with potassium hydroxide (1.0 g/L). The conductivity of the electrolytic solutions was determined on an MC226 conductivity meter (Mettler-Toledo). The positive and negative current density on the sample surface was predefined as $j_p = j_n = 6.0$ A/dm^2 by modulating the positive and negative voltages. The electrolyte composition, conductivity and relevant process electrical parameters were listed in Table 1. The temperature of the solutions was kept at 25–30 °C during the oxidation. Coated samples were flushed with water after the treatment and dried in warm air.

2.2. Coating structure and composition analyses

To evaluate fully the characteristics of oxide coatings, two groups of oxide coatings were produced in both electrolytes, namely thin coatings (Group 1) and thick coatings (Group 2). The treatment time and relevant thickness and roughness of the coatings were listed in Table 2. The thickness of the microarc oxidation coatings was measured with a MINITEST 1100 microprocessor coating thickness gauge (Elektro-physik Koln). The surface morphology and cross-section microstructure of the thick oxide coatings were observed with a JSM-5600LV scanning electron microscope (SEM). The surface roughness of the coatings was determined on a surface profilometer. The phase composition of the thick oxide coatings was analyzed by X-ray diffraction (XRD, X'Pert PRO), using Cu Kα radiation as the excitation source at a grazing angle of 2°.

Table 2
Thickness and surface roughness at different treatment time in two different electrolytes

Samples code	Electrolyte	Treatment time (min)	Coating thickness (μm)	Surface roughness (μm)
Group 1				
S1	Silicate	5	14	1.32
P1	Phosphate	5	13	1.20
Group 2				
S2	Silicate	30	37	2.24
P2	Phosphate	30	36.5	1.80

2.3. Mechanical and tribological evaluation

The outer porous layer of the thick oxide coatings was removed by abrasion against SiC paper. Then the microhardness of thick oxide coatings was evaluated by means of an MH-5 hardness tester with a Vicker indenter at a load of 25 g and for a loading duration of 5 s. The friction and wear properties of the microarc oxidation coatings sliding against Si_3N_4 ball of Ø 3 mm in a ball-on-disc configuration were evaluated on a reciprocal-sliding UMT-2MT tribometer (Center for Tribology, California, USA). The unlubricated sliding was performed at a load of 2 N with a sliding speed of 0.1 m/s and sliding amplitude of 5 mm at ambient temperature and humidity. A computer connected to the tester recorded the friction coefficient curves. Wear rates of oxide coatings were calculated by measuring the cross-sectional area of worn scar of the sample with a profilometer.

2.4. Corrosion testing

The corrosion resistance of the thick oxide coatings was determined by the potentiodynamic polarization tests using a CHI760B system, in which the samples with an exposed area of 0.24 cm^2 were immersed in a 3.5 wt.% NaCl solution. After 600 s of initial delay, the scanning was conducted with a constant rate of 10 mV/s from about −0.2 V versus an open circuit potential to approximately −1.0 V potential (referred to the SCE).

3. Results and discussion

3.1. Characteristics of voltage–time curves

Fig. 1 shows the dependencies of positive voltage on treatment time. According to the curves, four stages can be identified in both electrolytes. During the first 50–60 s (stage I), the voltage increases linearly in constant rate with time. In this stage, the Mg alloy substrate dissolves at first and loses its metal brightness, subsequently, a thin barrier layer is formed on the anode surface [13]. When the voltage exceeds a critical value, uniformly distributed small micro-sparks on the sample surfaces can be observed. The critical voltage corresponding to the appearance of micro-sparks on the sample surface is defined as the breakdown voltage, which has a strong dependence on the electrolytic composition and conductivity [14,15]. As shown in Table 1, the breakdown voltage in silicate

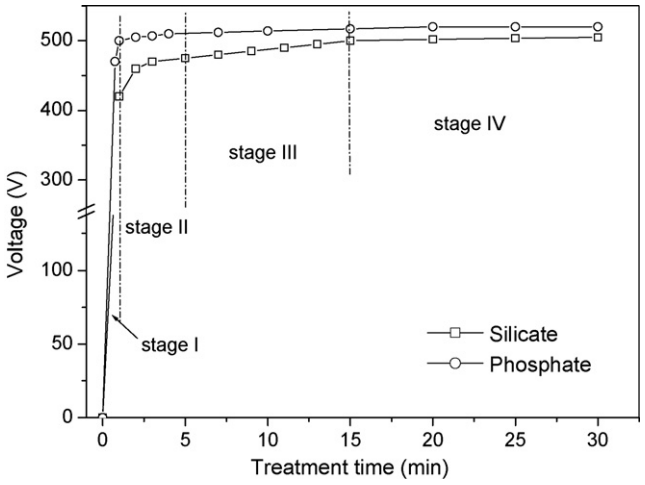

Fig. 1. Variations of positive voltages in different electrolytes: (□) positive voltage in Na_2SiO_3–KOH; (○) positive voltages in Na_3PO_4–KOH.

electrolyte (200 V) is smaller than that in phosphate electrolyte (255 V) during the MAO process. This can be attributed to the fact that silicate electrolyte has larger conductivity than that of phosphate electrolyte at the same mass concentration. In stage II, the rate of the increase in voltage reduces in both electrolytes at the same time. However, micro-sparks on the sample surfaces become more and larger than that in stage I. It is noted that the voltage in phosphate electrolyte is larger than that in silicate electrolyte under the same current density. In accordance with it, the number of micro-sparks on sample surfaces in phosphate electrolyte is larger than that in silicate electrolyte. After about 5 min of treatment, the process enters stage III and the slope of the curve $U = f(t)$ becomes smaller than stage II, where the appearance of the micro-sparks becomes more pronounced. The temporal duration of stage III is about 10 min in both electrolytes. Then, the process enters stage IV and the voltage is in a more steady-state, only changes in the appearance of micro-sparks are observed, which varies gradually from a dense population of small and frequent micro-sparks towards smaller population of relatively large and long-lived discharge events. In the 30 min treatment time, the final voltage in silicate electrolyte (505 V) is smaller than that in phosphate electrolyte (520 V).

3.2. Structure and composition of microarc oxidation coatings

Fig. 2 shows the surface and cross-section morphologies of the thick oxide coatings formed in two different electrolytes (samples S2 and P2). Fig. 2a and b demonstrates the differences in the surface of the coating formed in two electrolytes. Many micropores are found on top of both oxide coating surfaces and the size of the micropores ranges from 1 to 10 μm. In phosphate electrolyte, however, the oxide coating has more micropores than that formed in silicate electrolyte. Furthermore, SEM micrograph of the surface of coating formed in silicate electrolyte, as shown in Fig. 2a, exhibits the appearance of repeated and concentrated sintering and reveals a relatively coarse surface as compared with that of Fig. 2b. The differences

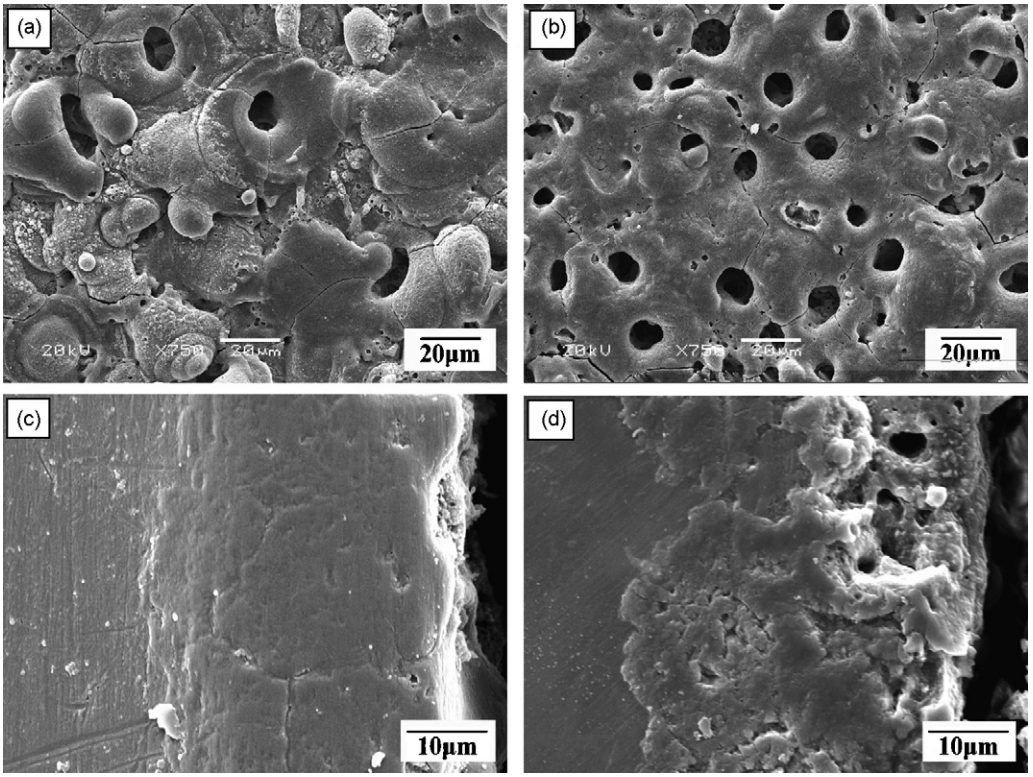

Fig. 2. SEM micrographs of surface and cross-section: (a and c) the coatings formed in silicate electrolyte (sample S2); (b and d) the coatings formed in phosphate electrolyte (sample P2).

of surface morphology of samples S2 and P2 are related to the characteristics of micro-sparks during the MAO process. The spark number in phosphate electrolyte is more than that in silicate electrolyte during the process, which leads to more micropores after the discharge channels are cooled. However, less micro-spark number in silicate electrolyte leads to an enhanced single discharge energy at the same current density [16]. Hence, the product mass by a single discharge is increased. When the melted product mass erupts from the discharge channel, it rapidly deposits around the discharge channels, thus, contributes to the appearance of repeated and concentrated sintering and the abnormity of micropores distribution. In accordance with it, the surface roughness listed in Table 2 also reveals that the coating formed in silicate electrolyte has a larger surface roughness than that formed in phosphate electrolyte.

The cross-section morphologies of samples S2 and P2 are shown in Fig. 2c and d. It is seen that sample S2 is more compact and uniform than that of sample P2, though both coatings has the similar thickness. Furthermore, the interface of coating and substrate of sample S2 is relatively more even compared to that of sample P2. It should be noted that there are not fracture sites in the interface of coating and substrate for both samples, indicating that the adhesion between the coating and substrate will be good.

XRD patterns of the thick oxide coatings are shown in Fig. 3. It can be seen that the coating formed in silicate electrolyte is composed of periclase MgO and forsterite Mg_2SiO_4 phases (Fig. 3a), while MgO and a little of spinel $MgAl_2O_4$ are the main phases of the coating formed in the phosphate electrolyte (Fig. 3b). The presence of Mg_2SiO_4 in sample S2 suggests that the SiO_3^{2-} anions in the electrolyte penetrate into discharge channels and react with the metal substrate during the microarc oxidation process. Unexpectedly, no peaks associated with phosphorus appear in the XRD pattern for sample P2, which indicates that phosphorus exists in the form of noncrystal phosphate type in the coating [17,18]. It is estimated that the instantaneous temperature in the micro-spark zone can reach several thousand degrees, thus the oxide products synthesized by plasma chemical interactions possess a stable chemical thermodynamic property [19,20].

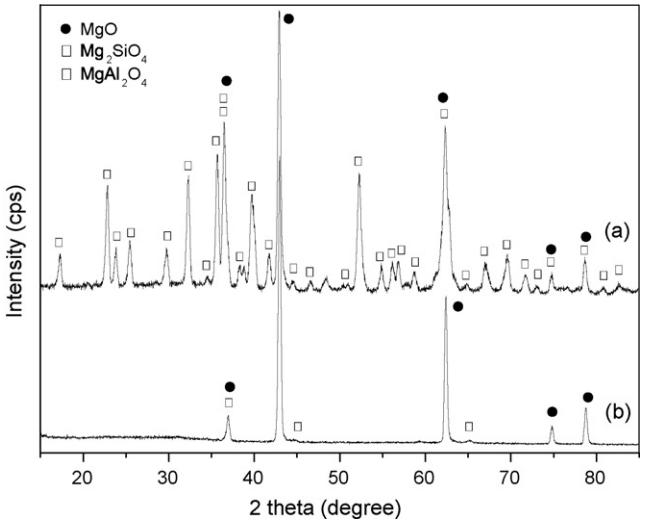

Fig. 3. XRD patterns of (a) sample S2 and (b) sample P2.

3.3. Mechanical and tribological properties

Fig. 4 shows the microhardness of the Mg alloy substrate and two types of MAO coatings prepared from the different electrolytes. It is seen that the microhardness of the oxide coatings is five to seven times higher than that of the Mg alloy substrate. Furthermore, the microhardness of sample S2 is higher than that of sample P2. This can be partly attributed to the fact that sample S2 has a more compact structure than that of sample P2. In addition, the different phase composition of the coating might also partly account for the higher microhardness of sample S2. Sample S2 consists of MgO and forsterite Mg_2SiO_4, while the main phase of sample P2 is MgO. Generally, the forsterite Mg_2SiO_4 has a greater hardness than that of the MgO [21]. Therefore, sample S2 exhibits a higher microhardness than sample P2.

The wear life of the oxide coatings formed in two different electrolytes is compared with the thin coatings (samples S1 and P1) and the results are shown in Fig. 5. The friction coefficients of both thin coatings are relatively high and stable before failure of the coatings. Once the coatings failed, the friction coefficients decrease about 0.3, which corresponds to the value of the uncoated sample [22]. Sample P1 is worn down around 600 s after starting the sliding test, as shown in Fig. 5, curve II. While sample S1 is able to last evidently longer (curve I) and the wear life is about four times as long as sample P1.

Fig. 6 demonstrates the evolution of the friction coefficients versus sliding time for the thick oxide coatings (samples S2 and P2). In addition, the friction coefficient of the substrate is also shown in this figure for the comparative purpose. Compared with the uncoated Mg alloy, the two coated samples register much larger friction coefficients as its slide against the ceramic ball under unlubricated condition. Sample S2 records a friction coefficient of 0.70–0.78, while sample P2 has a lower friction coefficient, which exhibits an average friction coefficient of

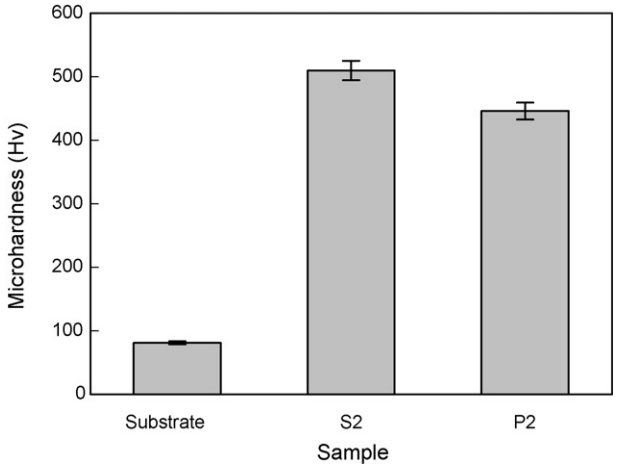

Fig. 4. Surface microhardness of the thick oxide coatings formed in different electrolytes.

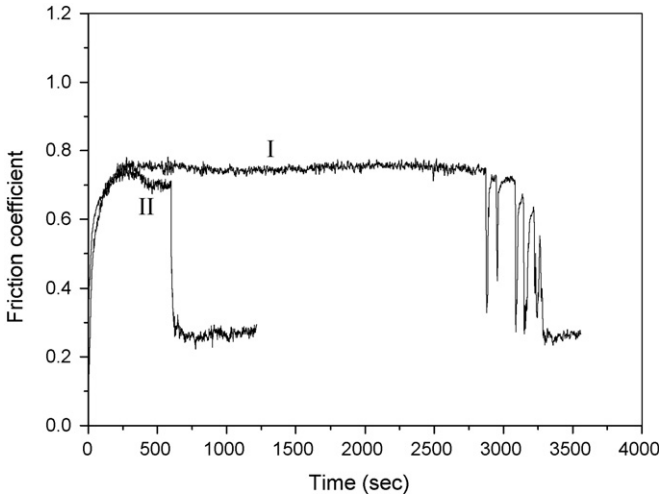

Fig. 5. Wear life of the thin oxide coatings with (curve I) the coating formed in silicate electrolyte (sample S1) and (curve II) the coating formed in phosphate electrolyte (sample P1).

0.60 in the steady state wear stage, though it increases slightly in the later stage. The difference of friction coefficients between samples S2 and P2 are attributed to the different microstructure and phase composition as mentioned above. Fig. 7 shows the wear rates of the uncoated Mg alloy and the two thick oxide coatings. The uncoated Mg alloy has a high wear rate of 3.81×10^{-4} mm^3/Nm, while the wear rates of both samples S2 and P2 are only in the range of $3.55–8.65 \times 10^{-5}$ mm^3/Nm, which indicates that the MAO coatings have much better wear resistance than the Mg alloy substrate. Furthermore, sample S2 has a better wear resistance than sample P1, though sample S2 has a higher friction coefficient during the sliding time. The enhancement of the wear resistance is due to the more compact structure and higher hardness of the coating prepared from the silicate electrolyte.

The difference in the friction behavior and wear rate of the two oxide coatings can be further verified by SEM photographs of wear tracks as shown in Fig. 8. It can be seen that both

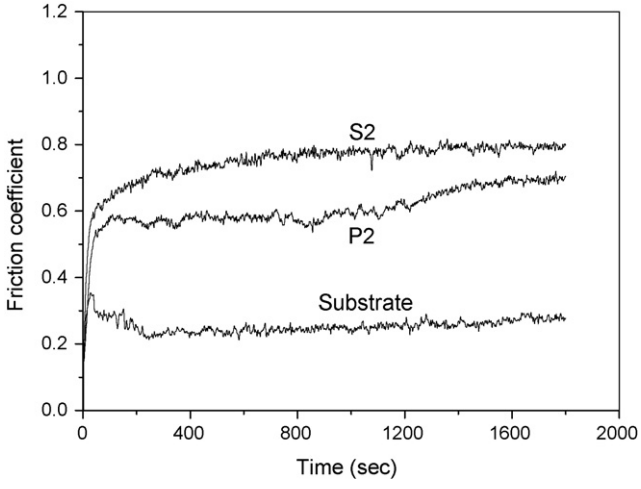

Fig. 6. Friction coefficients vs. sliding time for sample S2, sample P2 and the Mg alloy substrate.

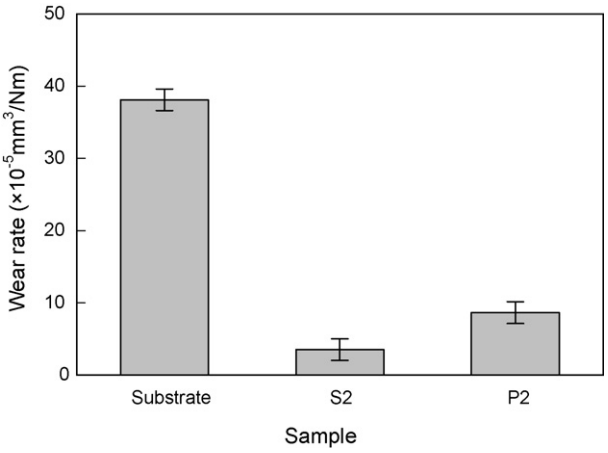

Fig. 7. Wear rates of the thick oxide coatings formed in different electrolytes and the Mg alloy substrate.

coatings are not penetrated during the test. For sample S2, the wear track (Fig. 8a) shows many non-continuous cracks. It suggests that surface fracture occurs when sliding against a Si_3N_4 ball, which results in a higher friction coefficient [23]. Compared with sample S2, the wear surface of sample P2 (Fig. 8b) exhibits a larger and smoother wear region, and the slight adhesive wear is the primary wear mechanism. These evidences demonstrate the fact that sample S2 has a higher friction coefficient but a better wear resistance than sample P2 has.

From these results, it can be concluded that the oxide coatings prepared from the silicate electrolyte have the better mechanical and tribological properties than that prepared from the phosphate electrolyte. It also suggests that the structure and phase composition of coatings are indeed the dominant factors which influence the mechanical property and friction and wear behavior of MAO coatings.

3.4. Anti-corrosion properties

The corrosion behavior of the coatings is evaluated by the electrochemical potentiodynamic polarization in a 3.5 wt.% NaCl solution. Fig. 9 demonstrates the potentiodynamic polarization curves of the coated samples formed in different electrolytes. The potentiodynamic polarization curve of the substrate is also given in this figure. The corrosion potential (E_{corr}) and the corrosion current density (i_{corr}) derived from the potentiodynamic polarization curves are shown in Table 3. The data clearly show that the enhanced corrosion protection was afforded by coatings. Both the coated samples S2 and P2 exhibit a more positive corrosion potential and a lower corrosion current density than the magnesium alloy substrate. Compared with the magnesium alloy substrate, the corrosion potential E_{corr} of the coating prepared from the silicate electrolyte increases by 87 mV, while the corrosion current density decreases by nearly two orders of magnitude. After the corrosion test, large corrosion craters can be clearly observed by the naked eye on the uncoated magnesium alloy surface. While for the coated samples, there is no visible change on the

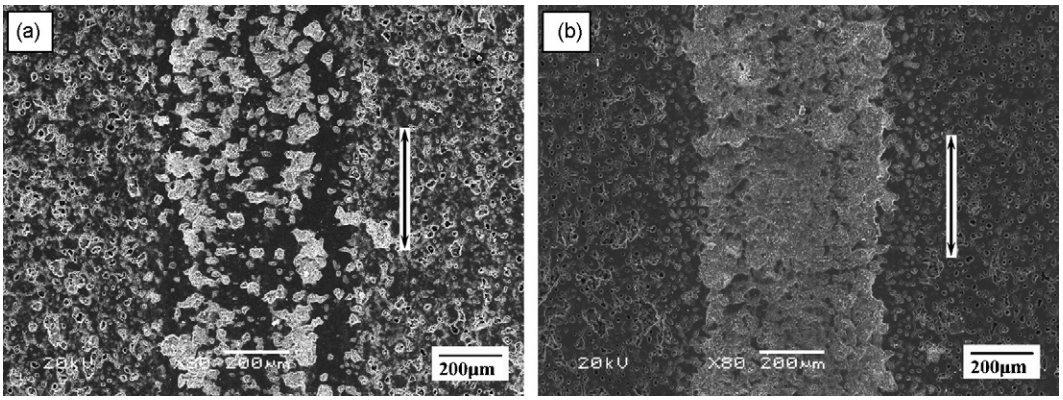

Fig. 8. SEM micrographs of wear tracks on the thick oxide coatings against Si_3N_4 ball: (a) sample S2; (b) sample P2. The arrows show the sliding directions.

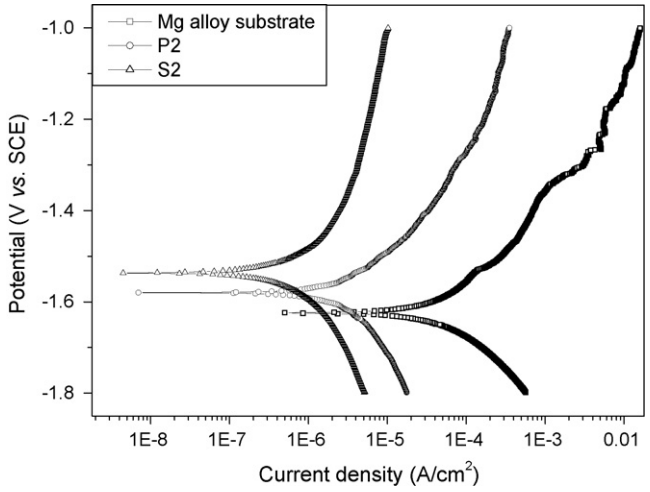

Fig. 9. Potentiodynamic polarization curves of the coatings formed in different electrolytes and the Mg alloy substrate in 3.5 wt.% NaCl solution.

coatings surface after corrosion testing. In contrast to samples S2 and P2, the coating prepared using a silicate electrolyte (sample S2) has a more positive corrosion potential (−1.537 V) and a lower corrosion current density (0.935 μA/cm^2) than sample P2 prepared from a phosphate electrolyte (−1.580 V and 4.212 μA/cm^2, respectively), indicating that it has a lower corrosion rate and a good corrosion resistance.

Above evidences illustrate that oxide coatings formed on magnesium alloys by microarc oxidation provide effective corrosion protective property for the substrate in solutions containing Cl^-. The superior corrosion protection provided by oxide coatings can be attributed to their relatively uniform, compact and intact microstructure as well as their relatively stable chemical thermodynamic composition [24].

Table 3
The results of potentiodynamic corrosion tests in 3.5 wt.% NaCl solution

	E_{corr} (V vs. SCE)	i_{corr} (μA/cm^2)
Substrate	−1.624	52.000
S2	−1.537	0.935
P2	−1.580	4.212

4. Conclusions

(1) Oxide coatings are formed on AM60B magnesium alloys by microarc oxidization in electrolytes containing silicate and phosphate at the constant applied current densities. Different electrolyte compositions cause the differences in the MAO processes, the values of breakdown voltage and the final voltage, and subsequently lead to differences in the characteristics of the oxide coating.
(2) The oxide coating formed in silicate electrolyte is compact and uniform and is mainly composed of MgO and forsterite Mg_2SiO_4 phases, while the coating formed in phosphate electrolyte is relatively porous and is mainly composed of MgO phase.
(3) The thick oxide coating formed in silicate electrolyte has a higher microhardness than that formed in phosphate electrolyte. Under dry sliding conditions, the wear rate of the former is approximately half that of the latter. However, the silicate coating exhibits a higher friction coefficient than the phosphate coating in the friction test.
(4) Both coatings produced in silicate and phosphate electrolytes provide effective protection for the corrosion resistance compared with the uncoated magnesium alloy, this is because they have compact microstructures and relatively stable thermodynamically chemical composition. The coating formed in silicate electrolyte has a better corrosion resistance property than that formed in phosphate electrolyte.

Acknowledgments

The financial support from the NSFC (Grant No. 50575218, L. Hu) is gratefully acknowledged. We thank Ms. L. He and Prof. J.Z. Zhao for their assistance in the experiments. The authors are also grateful to Mr. L.P. Wang for the instructive advice and discussion.

References

[1] E. Aghion, B. Bronfin, D. Eliezer, J. Mater. Process. Technol. 117 (2001) 381.

[2] J.E. Gray, B. Luan, J. Alloys Compd. 336 (2002) 88.
[3] N. Yamauchi, K. Demizu, N. Ueda, N.K. Cuong, T. Sone, Y. Hirose, Surf. Coat. Technol. 193 (2005) 277.
[4] D.E. Bartak, B.E. Lemieux, E.R. Woolsey, US Patent 5,264,113 (1993).
[5] O. Khaselev, D. Weiss, J. Yahalom, J. Electrochem. Soc. 146 (1999) 1757.
[6] A.L. Yerokhin, X. Nie, A. Leyland, A. Matthews, S.J. Dowey, Surf. Coat. Technol. 122 (1999) 73.
[7] A. Kuhn, Met. Finish. 101 (2003) 44.
[8] O. Khaselev, D. Weiss, J. Yahalom, Corros. Sci. 43 (2001) 1295.
[9] Y. Ma, X. Nie, D.O. Northwood, H. Hu, Thin Solid Films 469–470 (2004) 472.
[10] A.J. Zozulin, D.E. Bartak, Met. Finish. 92 (3) (1994) 39.
[11] F.A. Bonilla, A. Berkani, Y. Liu, P. Skeldon, G.E. Thompson, H. Habazaki, K. Shimizu, C. John, K. Stevens, J. Electrochem. Soc. 149 (2002) B4.
[12] V. Birss, S. Xia, R. Yue, R.G. Rateick Jr, J. Electrochem. Soc. 151 (2004) B1.
[13] L.O. Snizhko, A.L. Yerokhin, A. Pilkington, N.L. Gurevina, D.O. Misnyankin, A. Leyland, A. Matthews, Electrochim. Acta 49 (2004) 2085.
[14] S. Ikonopisov, Electrochim. Acta 22 (1977) 1077.
[15] J.M. Albella, I. Montero, J.M. Martínez-Duart, Electrochim. Acta 32 (1987) 255.
[16] Y.M. Wang, T.Q. Lei, B.L. Jiang, L.X. Guo, Appl. Surf. Sci. 233 (2004) 258.
[17] J. Liang, B.G. Guo, J. Tian, H.W. Liu, J.F. Zhou, W.M. Liu, T. Xu, Surf. Coat. Technol. 199 (2005) 121.
[18] H.Y. Hsiao, W.T. Tsai, Surf. Coat. Technol. 190 (2005) 299.
[19] A.L. Yerokhin, V.V. Lyubimov, R.V. Ashitkov, Ceram. Int. 122 (1999) 1.
[20] A.L. Yerokhin, A. Leyland, A. Matthews, Appl. Surf. Sci. 200 (2002) 172.
[21] Z.Q. Cai, L. Wang, G. Yang, Gradus of Ceramic Materials, Chemical Industry Publishing House, Beijing, 2001, pp. 171, 326 (in Chinese).
[22] J. Liang, B.G. Guo, J. Tian, H.W. Liu, J.F. Zhou, T. Xu, Appl. Surf. Sci. 252 (2005) 345.
[23] T.B. Wei, F.Y. Yan, W.M. Liu, J. Tian, Trans. Nonferrous Met. Soc. China 14 (6) (2004) 1162.
[24] Y.J. Zhang, C.W. Yan, F.H. Wang, H.Y. Lou, C.L. Cao, Surf. Coat. Technol. 161 (2002) 36.